IEEE Access
Multidisciplinary ⋮ Rapid Review ⋮ Open Access Journal

Received 25 June 2023, accepted 7 July 2023, date of publication 13 July 2023, date of current version 19 July 2023.

Digital Object Identifier 10.1109/ACCESS.2023.3294965

RESEARCH ARTICLE

Robust Sliding Mode Control With Optimal Path Following for Lateral Motion of Autonomous Bus

HUN HWANGBO[1], JAEUN RYU[2], SANGWON HAN[2], AND KUNSOO HUH[3], (Member, IEEE)
[1]Department of Future Mobility, Hanyang University, Seoul 04763, Republic of Korea
[2]Department of Automotive Engineering (Automotive-Computer Convergence), Hanyang University, Seoul 04763, Republic of Korea
[3]Department of Automotive Engineering, Hanyang University, Seoul 04763, Republic of Korea

Corresponding author: Kunsoo Huh (khuh2@hanyang.ac.kr)

This work was supported by the Technology Innovation Program (Industrial Strategic Technology Development Program, Development of Test Procedure Standards for Vehicle-to-Infrastructure (V2I) Connected Automated Driving Systems) funded by the Ministry of Trade, Industry and Energy (MOTIE), South Korea, under Grant 20014460.

ABSTRACT A robust and high-performance lateral control system is necessary for autonomous bus driving in complex downtown roads. In this paper, a Sliding Mode (SM) controller with an uncertainty observer is proposed to reduce the chattering phenomenon while ensuring robustness and maintaining the control performance. A stiffness gain is introduced in the cornering stiffness of rear wheels to compensate for the model uncertainty and external disturbance. For lane keeping and changing maneuvers, an optimal path planning algorithm is designed by considering dynamic constraints of the bus. The lane departure of bus is prevented with minimizing the lateral jerk through the sampling-based path regeneration process. The proposed lateral control system is compared to other conventional SM based controllers in the TRUCKSIM simulator. In an experiment with a real bus, lane keeping maneuver is conducted and compared with experienced human driver in the same driving course. Lane change maneuver is also tested with real bus to perform smooth lane transition while satisfying the lateral acceleration and yaw rate limitations.

INDEX TERMS Autonomous bus, lateral control system, sliding mode control, path planning, model uncertainty, stiffness gain.

I. INTRODUCTION

The Advanced Driving Assistant System (ADAS) technology has grown dramatically over the last decade, reducing driving fatigue and preventing traffic accidents. ADAS has evolved from partially assisting drivers to self-driving system that recognizes the surrounding environment, predicts future trajectories of nearby vehicles or pedestrians, and judges ongoing situation to create a safe driving path [1]. Recently, safety issues have been raised for the autonomous driving system [2], and the lateral motion control is particularly important in terms of safety of self-driving system [3]. It is necessary to minimize lateral position error from the lane centerline and discomfort of passengers while following the ever-changing driving path. In particular, autonomous bus driving in complex downtown must safely take an unspecified number of passengers to the designated stations, which require more sophisticated lateral control and path planning algorithms [4].

There are two models describing vehicle's lateral motion: kinematics-based and dynamics-based model, each with its own pros and cons [5]. The kinematic model assumes that the side slip of the vehicle is negligible. Early researchers developed a novel kinematics-based pure pursuit controller which is still widely used in lane keeping assistance system (LKAS) and self-driving system [6]. The pure pursuit uses simple geometric models and utilizes feedback of heading and lateral position errors from the sensors. Another research group developed a kinematics-based Stanley controller with calculating heading and lateral position errors from vehicle's front wheel axle [7]. Kinematics-based controllers enable simple but effective lateral control based on error feedback and do not need to know many vehicle parameters. However, the control performance deteriorates when the vehicle speed

The associate editor coordinating the review of this manuscript and approving it for publication was Jiujun Cheng.

increases in curvy road [8]. In addition, commercial vehicles like bus and truck have different number of wheels between front and rear axles, so the lateral movement caused by the difference in lateral forces between the front and rear axles should be considered [9].

The Dynamics-based lateral controller uses a dynamic model based on the Newton's second law. The side slip is considered and the control input can be designed according to the change of the vehicle parameters. In addition, the convergence of lateral position error and heading error can be proved mathematically so that stability of the controller is guaranteed [10]. But, the main weakness of dynamics-based controller is model uncertainty caused by unknown parameters such as cornering stiffness, mass, moment of inertia and center of gravity [11]. Especially, the cornering stiffness significantly varies depending on speed and vertical load. Each tire's vertical load is constantly changing as passengers get on and off, as bus accelerates or decelerates [12]. For these reasons, obtaining the precise value of the cornering stiffness is still an unsolved research topics [13]. Research has been conducted to overcome challenges in lateral control for buses. Shi et al. presents a robust path planning and tracking framework for autonomous buses, ensuring precise and resilient control in complex driving scenarios [14]. Han et al. proposed a CI-PI controller and collision avoidance trajectory planner for buses, considering vehicle stability and dynamic limitations [15].

Many controllers based on lateral dynamics have been developed to improve control performance while compensating model uncertainty. Marino et al. [16] developed dynamics-based two independent PID loops to minimize the lateral position and heading errors based on yaw rate from gyro sensor and vision sensor. Piao et al. proposes an LQR optimal controller for autonomous vehicle lateral control, improving trajectory tracking performance and system robustness [17]. Mohammadzadeh and Taghavifar [18] developed an adaptive estimator that estimates the cornering stiffness to minimize the model uncertainty. In [19], model uncertainty were estimated through extended state observer and the robustness against the change in the vehicle parameters was enhanced. Zhu et al. [20] designed a gain-scheduling technique that adjusts feedback gain and look-ahead distance according to the speed and weight. Jin et al. [21] introduced a nonlinear robust H_∞ state-feedback controller to consider model uncertainties in trajectory following performance.

Several studies using Model Predictive Control (MPC) have been conducted [22], [23], [24]. Lateral control using the MPC shows good control performance and can deal with model uncertainty. However, optimization-based control typically involves higher computation cost in comparison to other control techniques because the quadratic problem must be solved at every sampling time.

Sliding Mode Control (SMC) is an effective method for providing control robustness against model uncertainties. SMC has been used in scenarios where model parameters are constantly varying or nonlinearity exists in the model [25]. The SMC offers faster response time and lower computation cost than optimal control methods such as MPC or H_∞. Besides, the simplicity of the SMC allows it to be flexibly combined with a variety of control techniques to improve the system' robustness and performance, enabling specific requirements to be met [26]. Because real-time computation and performance robustness are crucial for path following control, the SMC is chosen as the most suitable for lateral control of autonomous buses.

Du et al. [27] mathematically proved stability of the SMC with the Lyapunov stability criteria and determined a steering angle which offset unknown disturbance and model uncertainty with high gain. In [28], the robustness of the controller was ensured using the super-twisting algorithm, and stability was proved through the backstepping technique. Norouzi et al. [29] reduced chattering by adjusting the boundary layer of the saturation function based on fuzzy logic such that the control input is changed smoothly to the size of the sliding surface. Since a SM-based lateral controller for bus [30] was introduced in 1996, few studies have been conducted to apply SMC to bus and demonstrate robustness and performance of controller on real-world roads.

In this study, SM-based lateral controller and an optimal path planning algorithm for bus are proposed. Using disturbance observer, model uncertainty in the dynamic model is estimated, which, in turn, updates the front and rear cornering stiffness. For lane keeping and lane change maneuvers, the optimization-based path planner creates an optimal trajectory first, and then the trajectory is re-planned by the search-based planner. The proposed path planning algorithm and controller are verified through commercial software. Experiments with real bus are conducted to verify the robustness of the proposed controller and the optimality of the path planner. The main contributions of this study are as follows:

1) Model uncertainties due to weight change and speed in bus are formulated as disturbance variables and they are estimated by using the disturbance observer.
2) Variations of the cornering stiffness at front and rear wheels are described as the stiffness gain with bias and they are updated in real time based on the estimated disturbance.
3) The sliding mode-based controller is formulated based on the estimated uncertainties and the updated model parameters to achieve the robust control performance in lateral motion of autonomous bus.
4) In order to improve driving safety and comfort of autonomous bus, the optimization-based and the search-based planners are combined to generate a trajectory that limits a lateral jerk and prevents lane departure.
5) The control performance for lane keeping and change maneuvers are verified not only in simulations, but also with real bus tests on the roads.

The contents of this paper is composed follows. Section II explains optimal path planning process and sampling-based

path regeneration algorithm. Section III describes lateral dynamics model and sliding mode controller design. The control performance and robustness to the model uncertainty are simulated in Section IV. Lane keeping and lane change tests in real roads are shown in Section V.

II. PATH PLANNER

Lateral control system for autonomous bus requires an optimal path that considers the dynamic constraints of bus. The lateral acceleration and jerk are the main causes of the passenger's ride discomfort and should be limited in the path planning process [31]. Excessive yaw rate should be also limited because it deteriorates the roll stability of the vehicle [32]. In addition, it is necessary to create a shortest path while satisfying dynamic constraints. Another important factor is to ensure that overhang does not deviate from the lane.

A. OPTIMIZATION-BASED PLANNER

The camera sensor or map server provides information on left-side and right-side lanes as 3rd order polynomials in the vehicle coordinate.

$$\begin{cases} f_L(x) = a_L x^3 + b_L x^2 + c_L x + d_L \\ f_R(x) = a_R x^3 + b_R x^2 + c_R x + d_R \end{cases} \tag{1}$$

where

$f_L(x)$: fitted function for the left-side lane
$f_R(x)$: fitted function for the right-side lane

By combining two functions, it is possible to obtain the lateral position and heading errors of the bus with respect to the lane centerline. In order to generate a path by considering displacement, speed, and acceleration, the path is expressed in a quintic function over time.

$$\begin{cases} x(t) = a_5 t^5 + a_4 t^4 + a_3 t^3 + a_2 t^2 + a_1 t + a_0 \\ y(t) = b_5 t^5 + b_4 t^4 + b_3 t^3 + b_2 t^2 + b_1 t + b_0 \end{cases} \tag{2}$$

To achieve autonomous driving for a specified distance within a given time limit, the longitudinal travel length (X_t) and travel time (T) from the initial time (t_0) to the final time (t_1) are chosen as design variables in optimization process [33]. It is assumed that the bus travels at constant velocity during the time span and the position of the bus at the target point is on the lane centerline. The lateral velocity and acceleration of the bus are expressed using the equations of the left lane and right lane. The overall boundary conditions for optimizing the quintic function are expressed in (3).

$$\begin{aligned} &x(t_0) = 0, \quad \dot{x}(t_0) = V_x, \quad \ddot{x}(t_0) = 0 \\ &x(t_1) = X_T, \quad \dot{x}(t_1) = V_x, \quad \ddot{x}(t_1) = 0 \\ &y(t_0) = y_{t_0}, \quad \dot{y}(t_0) = 0, \quad \ddot{y}(t_0) = 0 \\ &y(t_1) = y_{t_1}, \quad \dot{y}(t_1) = V_y, \quad \ddot{y}(t_1) = a_y \\ &T = t_1 - t_0 \end{aligned} \tag{3}$$

and

$$V_y = \frac{f'_L(X_T) + f'_R(X_T)}{2} \cdot \frac{\partial x}{\partial t}|_{t=t_1}$$
$$a_y = \frac{f''_L(X_T) + f''_R(X_T)}{2} \cdot \left(\frac{\partial x}{\partial t}|_{t=t_1}\right)^2$$

where

V_x : longitudinal velocity of the bus
V_y : lateral velocity at the target point
a_y : lateral acceleration at the target point
y_{t_0} : lateral position at the initial point
y_{t_1} : lateral position at the target point

Then $x(t)$ and $y(t)$ are expressed as function of T and X_T as follows.

$$\begin{cases} x(t) \to x(t, T, X_T, V_x) \\ y(t) \to y(t, T, X_T, V_y, a_y) \end{cases} \tag{4}$$

For a bus to follow the path with an acceptable lateral speed, the curvature of generated path must not be too large. The curvature for a specific time and the mean curvature for the entire travel time can be expressed as follows:

$$\kappa(t) = \left| \frac{\dot{x}(t) \cdot \ddot{y}(t) - \ddot{x}(t) \cdot \dot{y}(t)}{(\dot{x}(t)^2 + \dot{y}(t)^2)^{3/2}} \right|$$
$$\bar{\kappa} = \frac{\sum_{t_0}^{t_1} \kappa(t)}{n} \tag{5}$$

where

$\kappa(t)$: curvature for a specific time
$\bar{\kappa}$: mean curvature for the entire travel time
n : length of the time steps

The travel length from the current location to the target point can be expressed as in (6) over the entire travel time.

$$s = \sum_{t_0}^{t_f} \sqrt{\dot{x}(t)^2 + \dot{y}(t)^2} \tag{6}$$

Then, the cost function is selected to balance the mean of curvature and travel length as shown in (7). The travel length and travel time with the lowest cost maintain the driving efficiency while limiting excessive lateral movement.

$$J[X_T, T] = \omega_1 \bar{\kappa} + \omega_2 s \tag{7}$$

where ω_1 and ω_2 represent weights of the mean curvature and the travel length, respectively.

The constraints for lateral velocity and acceleration are experimentally set in the cost function.

$$\begin{cases} -2.5 m/s < \dot{y}(t) < 2.5 m/s \\ -0.5\, m/s^2 < \ddot{y}(t) < 0.5\, m/s^2 \end{cases} \tag{8}$$

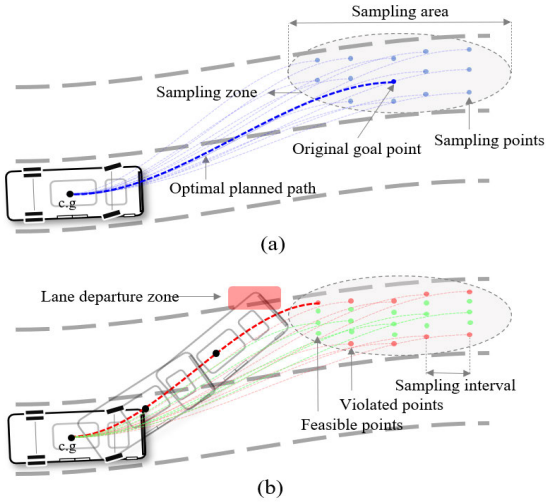

FIGURE 1. Sampling based path planning (a) Candidate goal points (b) Feasible paths and discarded paths.

In order to satisfy the yaw stability for bus, the yaw rate must be limited. Equation (9) describes the expression of yaw rate and its constraint of a given path.

$$\dot{\psi}(t) = \frac{\dot{x}(t) \cdot \ddot{y}(t) - \ddot{x}(t) \cdot \dot{y}(t)}{\dot{x}^2(t) + \dot{y}^2(t)} \tag{9}$$

and

$$-0.1\, rad/s < \dot{\psi}(t) < 0.1\, rad/s$$

where $\dot{\psi}(t)$ is yaw rate of the bus.

The cost function under constraints (8) and (9) is solved by the quadratic problem solver [34]. The inputs to the optimization algorithm are the current speed, lateral offset at the initial time, and lateral offset, lateral speed and acceleration at the time of arrival. The optimized outputs are longitudinal travel length and travel time.

B. SEARCH-BASED PLANNER

Because the bus has larger width and front-overhang than passenger car, its lane keeping should be carefully considered. The path obtained from the optimization-based planner is rerouted in order to operate at minimum lateral jerk and not to depart from the lane [35]. First, several goal points are additionally generated as shown in Fig.1 by applying offset at regular intervals from the original goal point which was obtained from the optimization-based planner. For each goal point, the 5^{th} polynomial path is generated by the optimization-based planner. Secondly, paths that may deviate from the lane are removed. The goal point of the final path should maintain a minimum lateral offset with the minimized lateral jerk. The second cost function is designed to balance between the requirements at the same time. Lastly, the cost values of the remaining feasible paths are obtained and the final path with the lowest cost value is selected as shown in Fig.2.

$$J_{traj,i} = \omega_{jerk} \sum_{t=0}^{T} \left|\dddot{y}_i(t)\right| + \omega_{center} \left\|P_i - P_{center}\right\| \tag{10}$$

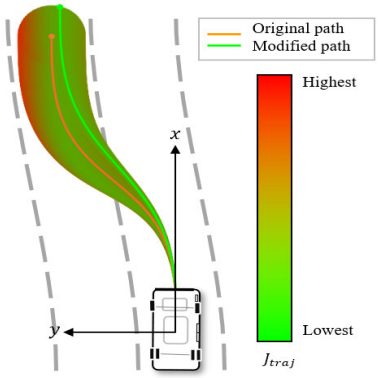

FIGURE 2. Original path and rerouted path.

where

P_{center} : the original goal point (x, y)
P_i : candidate goal points
$\omega_{jerk}, \omega_{center}$: the constant weight factors

III. LATERAL CONTROLLER DESIGN

A. LATERAL VEHICLE DYNAMICS MODEL

The lateral motion of the bus is represented by a bicycle model where two wheels at the front and rear axles are summed to one wheel, respectively, as illustrated in Fig. 4. Because the moderate maneuvering is expected based on the generated path in Section II, the lateral tire force at each tire is assumed proportional to the corresponding slip angle as shown in equation (11) [10].

$$\begin{cases} F_{yf} = 2C_{\alpha f}\left(\delta - \dfrac{\dot{y} + l_f\dot{\psi}}{V_x}\right) \\ F_{yr} = -2C_{\alpha r}\left(\dfrac{\dot{y} - l_r\dot{\psi}}{V_x}\right) \end{cases} \tag{11}$$

where $C_{\alpha f}$: cornering stiffness of front tire
$C_{\alpha r}$: cornering stiffness of rear tire
l_f : distance between front axle and center of gravity
l_r : distance between rear axle and center of gravity
δ : front steering angle
F_{yf} : lateral force of front axle
F_{yr} : lateral force of rear axle

The cornering stiffness in (11) varies significantly depending on vehicle speed, vertical load of tires, etc., which is considered in this study. In particular, the cornering stiffness at front and rear tires are assumed to have bias and time varying gain as expressed in equation (16). By doing so, the nonlinear tire characteristics are approximated by the

estimated uncertainties in bias and gain. The uncertainties arising from such nonlinearity are estimated by the uncertainty observer later in the next section. Fig.3 describes the error variables of the bus with respect to the desired path. e_1 represents the lateral distance from the centerline to the vehicle's center of gravity. e_2 represents the heading error between the tangent line of the desired path and the vehicle's heading vector. The state-space model for the error variables is derived from the bicycle model [10].

$$\frac{d}{dt}\begin{bmatrix} e_1 \\ \dot{e}_1 \\ e_2 \\ \dot{e}_2 \end{bmatrix} = \begin{bmatrix} 0 & 1 & 0 & 0 \\ 0 & a_{22} & a_{23} & a_{24} \\ 0 & 0 & 0 & 1 \\ 0 & a_{42} & a_{43} & a_{44} \end{bmatrix} \begin{bmatrix} e_1 \\ \dot{e}_1 \\ e_2 \\ \dot{e}_2 \end{bmatrix} + \begin{bmatrix} 0 \\ b_2 \\ 0 \\ b_4 \end{bmatrix} \delta + \begin{bmatrix} 0 \\ c_2 \\ 0 \\ c_4 \end{bmatrix} \dot{\psi}_d \tag{12}$$

where

$$a_{22} = -\frac{2C_{af} + 2C_{ar}}{mV_x}, \quad a_{23} = \frac{2C_{af} + 2C_{ar}}{m},$$
$$a_{24} = \frac{2C_{af}l_f + 2C_{ar}l_r}{mV_x}, \quad a_{42} = -\frac{2C_{af}l_f - 2C_{ar}l_r}{I_zV_x},$$
$$a_{43} = \frac{2C_{af}l_f - 2C_{ar}l_r}{I_z}, \quad a_{44} = -\frac{2C_{af}l_f^2 + 2C_{ar}l_r^2}{I_zV_x},$$
$$b_2 = \frac{2C_{af}}{m}, \quad b_4 = \frac{2C_{af}l_f}{I_z},$$
$$c_2 = -\frac{2C_{af}l_f + 2C_{ar}l_r}{mV_x} - V_x, \quad c_4 = -\frac{2C_{af}l_f^2 + 2C_{ar}l_r^2}{I_zV_x}$$

B. UNCERTAINTY ANALYSIS AND DISTURBANCE OBSERVER DESIGN

For a bus, several parameters in (12) can change depending on the driving conditions. For example, mass of the bus can change significantly with a large number of passengers, which, in turn, changes the moment of inertia and the cornering stiffness of tires. Besides, the initial value of the cornering stiffness may not be accurate. The initial uncertainties of the cornering stiffness and the changes of the vehicle parameters are expressed as follows:

$$\begin{aligned}\ddot{e}_1 = &- \frac{2k_{C\alpha f}(\bar{C}_{\alpha f} + \Delta C_{\alpha f}) + 2k_{C\alpha r}(\bar{C}_{\alpha r} + \Delta C_{\alpha r})}{k_m\bar{m}V_x} \cdot \dot{e}_1 \\ &+ \frac{2k_{C\alpha f}(\bar{C}_{\alpha f} + \Delta C_{\alpha f}) + 2k_{C\alpha r}(\bar{C}_{\alpha r} + \Delta C_{\alpha r})}{k_m\bar{m}} \cdot e_2 \\ &- \frac{2k_{C\alpha f}(\bar{C}_{\alpha f} + \Delta C_{\alpha f})l_f + 2k_{C\alpha r}(\bar{C}_{\alpha r} + \Delta C_{\alpha r})l_r}{k_m\bar{m}V_x} \cdot \dot{e}_2 \\ &- \frac{2k_{C\alpha f}(\bar{C}_{\alpha f} + \Delta C_{\alpha f})l_f + 2k_{C\alpha r}(\bar{C}_{\alpha r} + \Delta C_{\alpha r})l_r}{k_m\bar{m}V_x} \cdot \dot{\psi}_d \\ &+ \frac{2k_{C\alpha f}(\bar{C}_{\alpha f} + \Delta C_{\alpha f})}{k_m\bar{m}V_x} \cdot \delta \end{aligned} \tag{13}$$

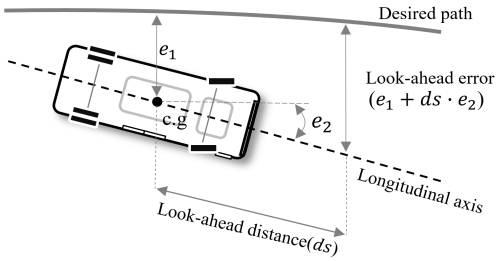

FIGURE 3. Error variables based on road centerline.

$$\begin{aligned}\ddot{e}_2 = &+ \frac{-2k_{C\alpha f}(\bar{C}_{\alpha f} + \Delta C_{\alpha f})l_f + 2k_{C\alpha r}(\bar{C}_{\alpha r} + \Delta C_{\alpha r})l_r}{k_I\bar{I}_zV_x} \cdot \dot{e}_1 \\ &+ \frac{2k_{C\alpha f}(\bar{C}_{\alpha f} + \Delta C_{\alpha f})l_f - 2k_{C\alpha r}(\bar{C}_{\alpha r} + \Delta C_{\alpha r})l_r}{k_I\bar{I}_z} \cdot e_2 \\ &- \frac{2k_{C\alpha f}(\bar{C}_{\alpha f} + \Delta C_{\alpha f})l_f^2 + 2k_{C\alpha r}(\bar{C}_{\alpha r} + \Delta C_{\alpha r})l_r^2}{k_I\bar{I}_zV_x} \cdot \dot{e}_2 \\ &- \frac{2k_{C\alpha f}(\bar{C}_{\alpha f} + \Delta C_{\alpha f})l_f^2 + 2k_{C\alpha r}(\bar{C}_{\alpha r} + \Delta C_{\alpha r})l_r^2}{k_I\bar{I}_zV_x} \cdot \dot{\psi}_d \\ &+ \frac{2k_{C\alpha f}(\bar{C}_{\alpha f} + \Delta C_{\alpha f})l_f}{k_I\bar{I}_z} \cdot \delta \end{aligned} \tag{14}$$

In (13), parameters with bar represent the initial values known from the vehicle specifications. Parameters with delta(Δ) mean bias in the initial values. The coefficient, k, at each parameter indicate changes in parameter values over time. During the moderate cornering(e.g. slip angle is less than 4°), three parameters of mass, moment of inertia and the cornering stiffness change approximately in proportion [36], [37]. Thus, the coefficients for the three parameters are assumed to have the similar size.

$$k_m \simeq k_{Iz} \simeq k_{C\alpha f} \simeq k_{C\alpha r} \tag{15}$$

Unlike mass and moment of inertia, the initial value of the cornering stiffness may not be accurate in real situations. The rear wheels of bus should carry a larger load than the front wheels and the capacity of the lateral force at rear wheels should be enhanced for stability. The rear cornering stiffness is always greater than the front cornering stiffness and the stiffness gain is introduced in this study. Then, variations of the front and rear cornering stiffness are expressed as follows:

$$\begin{cases} C_{af} = \bar{C}_{af} + \Delta C_{af} \\ C_{ar} = C_{af} \cdot k_c \end{cases} \tag{16}$$

where

k_c : stiffness gain

ΔC_{af} : bias of the front cornering stiffness

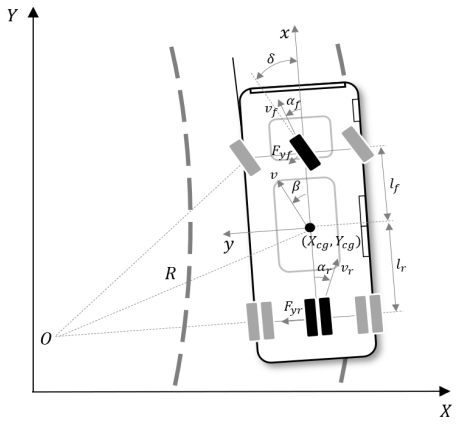

FIGURE 4. Bicycle model for lateral motion of bus.

Then, the state space model can be rewritten by utilizing (15) and (16).

$$\frac{d}{dt}\begin{bmatrix} e_1 \\ \dot{e}_1 \\ e_2 \\ \dot{e}_2 \end{bmatrix} = \begin{bmatrix} 0 & 1 & 0 & 0 \\ 0 & \bar{a}_{22}+\Delta a_{22} & \bar{a}_{23}+\Delta a_{23} & \bar{a}_{24}+\Delta a_{24} \\ 0 & 0 & 0 & 1 \\ 0 & \bar{a}_{42}+\Delta a_{42} & \bar{a}_{43}+\Delta a_{43} & \bar{a}_{44}+\Delta a_{44} \end{bmatrix}\begin{bmatrix} e_1 \\ \dot{e}_1 \\ e_2 \\ \dot{e}_2 \end{bmatrix} + \begin{bmatrix} 0 \\ \bar{b}_2+\Delta b_2 \\ 0 \\ \bar{b}_4+\Delta b_4 \end{bmatrix}\delta + \begin{bmatrix} 0 \\ \bar{c}_2+\Delta c_2 \\ 0 \\ \bar{c}_4+\Delta c_4 \end{bmatrix}\dot{\psi}_d \tag{17}$$

The parameters in (17) are described in detail in the appendix A. The second derivatives of e_1 and e_2 are rewritten by grouping the Δ parameters as a total disturbance term.

$$\begin{cases} \ddot{e}_1 = \bar{a}_{22}\dot{e}_1 + \bar{a}_{23}e_2 + \bar{a}_{24}\dot{e}_2 + \bar{b}_2\delta + \bar{c}_2\dot{\psi}_d + f_1 \\ \ddot{e}_2 = \bar{a}_{42}\dot{e}_1 + \bar{a}_{43}e_2 + \bar{a}_{44}\dot{e}_2 + \bar{b}_4\delta + \bar{c}_4\dot{\psi}_d + f_2 \end{cases} \tag{18}$$

where

$$f_1 = \Delta a_{22}\dot{e}_1 + \Delta a_{23}e_2 + \Delta a_{24}\dot{e}_2 + \Delta b_2\delta + \Delta c_2\dot{\psi}_d$$
$$f_2 = \Delta a_{42}\dot{e}_1 + \Delta a_{43}e_2 + \Delta a_{44}\dot{e}_2 + \Delta b_4\delta + \Delta c_4\dot{\psi}_d$$

By substituting the detailed expression for Δ parameters, the disturbance terms, f_1 and f_2, can be expressed by $\Delta C_{\alpha f}$ and k_c as follows:

$$\begin{cases} f_1 = 2\Delta C_{\alpha f}(-\frac{1}{mV_x}\dot{e}_1 + \frac{1}{m}e_2 - \frac{l_f}{mV_x}\dot{e}_2 + \frac{1}{m}\delta \\ \quad -\frac{l_f}{mV_x}\dot{\psi}_d + k_c(-\frac{1}{mV_x}\dot{e}_1 + \frac{1}{m}e_2 + \frac{l_r}{mV_x}\dot{e}_2 + \frac{l_r}{mV_x}\dot{\psi}_d)) \\ f_2 = 2\Delta C_{\alpha f}(-\frac{l_f}{I_zV_x}\dot{e}_1 + \frac{l_f}{I_z}e_2 - \frac{{l_f}^2}{I_zV_x}\dot{e}_2 + \frac{l_f}{I_z}\delta \\ \quad -\frac{{l_f}^2}{I_zV_x}\dot{\psi}_d + k_c(\frac{l_r}{I_zV_x}\dot{e}_1 - \frac{l_r}{I_z}e_2 - \frac{{l_r}^2}{I_zV_x}\dot{e}_2 - \frac{{l_r}^2}{I_zV_x}\dot{\psi}_d)) \end{cases} \tag{19}$$

Then, the two equations in (20) can be solved for $\Delta C_{\alpha f}$ and k_c.

$$k_c = \frac{\Theta f_2 - \Pi f_1}{\Phi f_1 - \Xi f_2}$$
$$\Delta C_{\alpha f} = \frac{f_1}{\Theta + \Xi k_c} \tag{20}$$

where

$$\Theta = -\frac{2}{mV_x}\dot{e}_1 + \frac{2}{m}e_2 - \frac{2l_f}{mV_x}\dot{e}_2 + \frac{2}{m}\delta - \frac{2l_f}{mV_x}\dot{\psi}_d$$
$$\Pi = -\frac{2l_f}{I_zV_x}\dot{e}_1 + \frac{2l_f}{I_z}e_2 - \frac{2{l_f}^2}{I_zV_x}\dot{e}_2 + \frac{2l_f}{I_z}\delta - \frac{2{l_f}^2}{I_zV_x}\dot{\psi}_d$$
$$\Phi = \frac{2l_r}{I_zV_x}\dot{e}_1 - \frac{2l_r}{I_z}e_2 - \frac{2{l_r}^2}{I_zV_x}\dot{e}_2 - \frac{2{l_r}^2}{I_zV_x}\dot{\psi}_d$$
$$\Xi = -\frac{2}{mV_x}\dot{e}_1 + \frac{2}{m}e_2 + \frac{2l_r}{mV_x}\dot{e}_2 + \frac{2l_r}{mV_x}\dot{\psi}_d$$

If f_1 and f_2 can be estimated, k_c and $\Delta C_{\alpha f}$ are calculated using (20) and their values are used to update the cornering stiffness based on (16).

A disturbance observer is designed for estimating f_1 and f_2 by assuming that the disturbance is observable with slowly time-varying condition [38].

$$\dot{f}_1 \simeq \delta_1$$
$$\dot{f}_2 \simeq \delta_2 \tag{21}$$

where δ_1 and δ_2 are constant values.

Equation (18) can be used to calculate f_1 and f_2 as the initial measurement based on the nominal parameter values and the sensor values.

$$\begin{cases} f_1 = \ddot{e}_1 - \bar{a}_{22}\dot{e}_1 - \bar{a}_{23}e_2 - \bar{a}_{24}\dot{e}_2 - \bar{c}_2\dot{\psi}_d - \bar{b}_2\delta \\ f_2 = \ddot{e}_2 - \bar{a}_{42}\dot{e}_1 - \bar{a}_{43}e_2 - \bar{a}_{44}\dot{e}_2 - \bar{c}_4\dot{\psi}_d - \bar{b}_4\delta \end{cases} \tag{22}$$

A PI (Proportional/Integral) disturbance observer [38] is utilized to estimate the disturbances.

$$\begin{cases} \dot{\hat{f}}_1 = l_1(f_1 - \hat{f}_1) + l_2 \cdot \int (f_1 - \hat{f}_1)dt \\ \dot{\hat{f}}_2 = l_3(f_2 - \hat{f}_2) + l_4 \cdot \int (f_2 - \hat{f}_2)dt \end{cases} \tag{23}$$

where

$\hat{f}_1$: estimate of f_1
$\hat{f}_2$: estimate of f_2
l_1, l_2, l_3, l_4 : observer gains

Then, the estimation error for f_1 can be expressed as follows:

$$\dot{\tilde{f}}_1 = -l_1\tilde{f}_1 - l_2\int \tilde{f}_1 + \dot{f}_1 \tag{24}$$

where

$$\tilde{f}_1 = f_1 - \hat{f}_1$$

By differentiating (24) and using the assumption of (21), the estimation error dynamics are governed by the equation.

$$\ddot{\tilde{f}}_1 + l_1\dot{\tilde{f}}_1 + l_2\tilde{f}_1 = 0$$
$$\text{or } (s^2 + l_1 s + l_2)\tilde{F}_1(s) = 0 \tag{25}$$

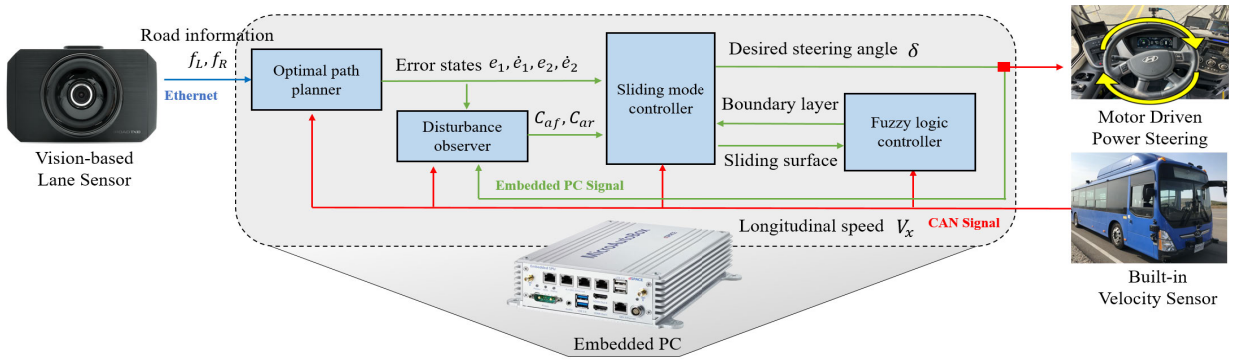

FIGURE 5. Overall architecture of the proposed control system.

With positive observer gains, Hurwitz stability is satisfied because the poles of the error dynamics are placed on the left side pole plane [38]. The convergence of $\tilde{f}_2$ can be also proved in the same way as $\tilde{f}_1$. Thus, it can be proved that the estimation errors for both disturbances converge to zero.

C. CONTROLLER DESIGN

The Sliding Mode Controller (SMC) is designed based on the lateral dynamics model in (12) where the cornering stiffness at front and rear wheels are updated as explained in the previous section. Figure 5 shows the overall architecture of the proposed lateral control system. The lane sensor transmits lane information to the Embedded PC through the Ethernet and the Path Planner calculates the vehicle's future trajectory. The Controller determines the required steering angle based on the error states and the estimated cornering stiffness. The calculated steering angle is then sent to the Motor Driven Power Steering (MDPS) module via the CAN network. The real-time speed of the vehicle is obtained through a built-in velocity sensor and transmitted to the Embedded PC via the CAN network

For the SMC design, the sliding surface is set as shown in (26) for the bus to stay centered in the occupied lane while aligning the heading angle with the centerline direction.

$$\begin{aligned} e &= e_1 + ds \cdot e_2 \\ s &= \dot{e} + \lambda e \end{aligned} \tag{26}$$

where λ is sliding slope.

The Lyapunov function is selected as (27) and its derivative can be expressed as follows:

$$\begin{aligned} V &= \frac{1}{2}s^2 \\ \dot{V} &= s \cdot \dot{s} \\ &= s(\ddot{e} + \lambda \dot{e}) \\ &= s(\dot{e}_1(a_{22} + ds \cdot a_{42} + \lambda) + e_2(a_{23} + ds \cdot a_{43}) \\ &\quad + \dot{e}_2(a_{24} + ds \cdot a_{44} + \lambda \cdot ds) + \delta(b_2 + ds \cdot b_4) \\ &\quad + \dot{\psi}_d(c_2 + ds \cdot c_4)) \end{aligned} \tag{27}$$

If the control input is set as follows:

$$\begin{aligned} \delta = (b_2 + ds \cdot b_4)^{-1}(&-\dot{e}_1(a_{22} + ds \cdot a_{42} + \lambda) \\ &-\dot{e}_2(a_{24} + ds \cdot a_{44} + \lambda \cdot ds) - e_2(a_{23} + ds \cdot a_{43}) \\ &-\dot{\psi}_d(c_2 + ds \cdot c_4) - \eta \cdot sign(s)) \end{aligned} \tag{28}$$

where η is SMC gain, the Lyapunov stability condition is satisfied and the convergence of the error is guaranteed [26].

$$\dot{V} = -\eta\,|s| \leq 0 \tag{29}$$

In this study, the uncertain parameters such as cornering stiffness in (12) are updated in advance using the disturbance observer, a small SMC gain can be used to compensate the uncertainties. Nonetheless, a little chattering can still exisit and signum function is replaced with saturation function to minimize chattering and to resolve the discontinuity in signum function. In addition, in order to improve the control performance, Fuzzy logic [39] is applied to make boundary layer change to the sliding surface and velocity. As shown in Fig.6, five membership functions are set for s and V_x. The centroid technique is used as the defuzzification method and the output membership function is described in Fig.7. Table 1 shows the rule by which the output membership function is determined based on sliding surface and velocity.

Besides, SMC gain is selected to change according to the sliding surface [40] to improve the control performance. The SMC gain is increased in the reaching phase and reduced in the sliding phase.

$$\eta(s) = \rho \cdot |s|^{1/2} \tag{30}$$

where ρ is gain constant.

Then, the steering angle from the SMC controller is in the following form considering the fuzzy boundary layer and adaptive sliding mode gain.

$$\begin{aligned} \delta = (b_2 + ds \cdot b_4)^{-1}(&-\dot{e}_1(a_{22} + ds \cdot a_{42} + \lambda) \\ &-\dot{e}_2(a_{24} + ds \cdot a_{44} + \lambda \cdot ds) - e_2(a_{23} + ds \cdot c_4) \\ &-\dot{\psi}_{des}(c_2 + ds \cdot c_4) - (\rho \cdot |s|^{1/2}) \cdot sat(\frac{s}{\phi(s, V_x)})) \end{aligned} \tag{31}$$

where $\phi(s, V_x)$ is adaptive boundary layer.

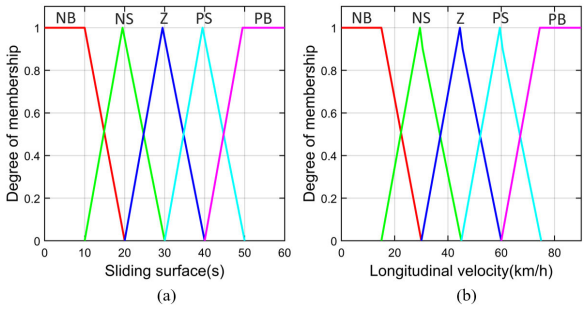

FIGURE 6. Fuzzified input variables (a) Membership functions of sliding surface. (b) Membership functions of longitudinal velocity.

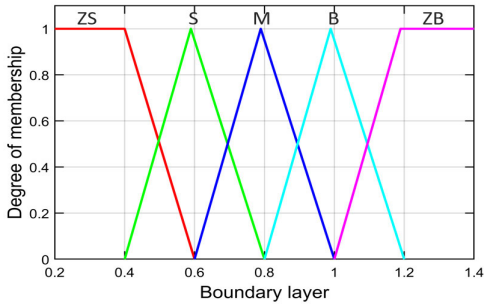

FIGURE 7. Output membership functions of boundary layer.

From the perspective of lane keeping or path following control, an additional constraint conditions can be obtained for the stiffness gain in (16). The controlled steering angle in (31) is expressed in the negative feedback form from $\dot{e}_1$, e_2, and $\dot{e}_2$. Thus, the coefficient of each term should have a positive value to move to the opposite direction of the errors in lateral offset error and heading error.

$$\begin{cases} a_{22} + ds \cdot a_{42} + \lambda > 0 \\ a_{24} + ds \cdot a_{44} + \lambda \cdot ds > 0 \\ a_{23} + ds \cdot c_4 > 0 \end{cases} \tag{32}$$

The above inequality equations in (32) can be solved for the stiffness gain and the constraint conditions are obtained in (33). The stiffness gain calculated by (20) must be between the upper and lower bounds in (33).

$$\begin{aligned} k_c &> (\frac{1}{mV_x} + ds \cdot \frac{l_f}{I_z V_x} - \frac{\lambda}{2C_{af}})/(-\frac{1}{mV_x} + ds \cdot \frac{l_r}{I_z V_x}) \\ k_c &< (\frac{l_f}{mV_x} + ds \cdot \frac{{l_f}^2}{I_z V_x} - \frac{\lambda \cdot ds}{2C_{af}})/(\frac{l_r}{mV_x} - ds \cdot \frac{{l_r}^2}{I_z V_x}) \\ k_c &< (\frac{1}{m} + ds \cdot \frac{l_f}{I_z})/(-\frac{1}{m} + ds \cdot \frac{l_r}{I_z}) \end{aligned} \tag{33}$$

IV. SIMULATION

The TRUCKSIM software [41] is used to compare the performance of three SM-based lateral controllers. Fig.8 shows the driving track and road scene of the simulation environment.

The longitudinal speed is set to 50 km/h and the driving track is composed of two curves with radius of 150 m and 120 m. The nominal parameter values of the bus are listed in Table 2.

Table 3 summarizes the characteristics of the conventional SM controllers and the proposed SM controller. The constant SMC [27] utilizes the continuous approximation of *signum* function to converge the sliding surface to zero and requires a high SMC gain to overcome model uncertainty and external disturbance. The adaptive SMC [29] reduces chattering by

TABLE 1. Basic rules of the fuzzy boundary layer.

		Sliding surface				
		NB	NS	Z	PS	PB
V_x	NB	ZB	ZB	B	B	M
	NS	ZB	B	B	M	S
	Z	B	B	M	S	S
	PS	B	M	S	S	ZS
	PB	M	S	S	ZS	ZS

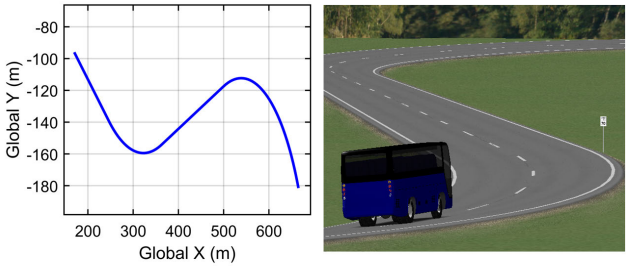

FIGURE 8. TRUCKSIM simulation environment (a) Driving track (b) Graphical scene.

TABLE 2. Bus parameters in simulation.

Symbol	Value	Unit
m	7200	kg
I_z	30782	$kg \cdot m^2$
l_f	3.15	m
l_r	4.95	m
$C_{\alpha f}$	128925	N/rad
$C_{\alpha r}$	186225	N/rad

TABLE 3. Main differences of SM-based controllers.

	Constant SMC [27]	Adaptive SMC [29]	Proposed SMC
SMC input	$\frac{\eta}{B} \cdot (\frac{s}{\lvert s \rvert + \varepsilon})$	$\frac{\eta(s)}{B} \cdot sat(\frac{s}{\phi(s)})$	$\frac{\eta(s)}{B} \cdot sat(\frac{s}{\phi(s, V_x)})$
$C_{\alpha f}$	128925	128925	128925 + $\Delta C_{\alpha f}$
$C_{\alpha r}$	186225	186225	$C_{\alpha f} \cdot k_c$

TABLE 4. Gain parameters of the proposed SMC.

Symbol	Value	Symbol	Value
l_1	30	l_4	1
l_2	1	λ	3
l_3	30	ρ	0.5

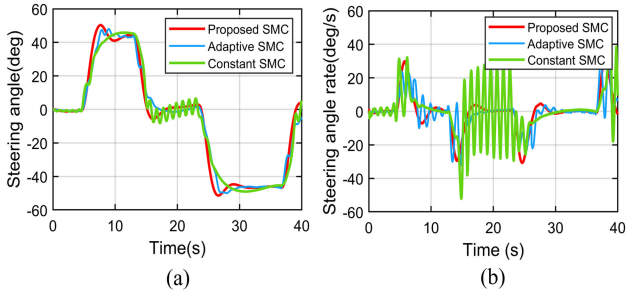

FIGURE 9. Steering angle and steering rate.

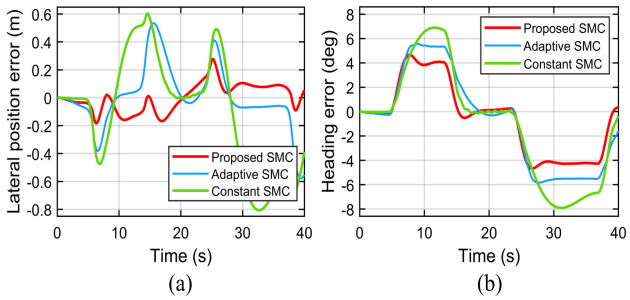

FIGURE 10. Lateral offset error and heading error.

using fuzzy logic and by making SMC gain proportional to the sliding surface, but does not use the disturbance estimation suggested in this study. The gain parameters of the proposed SMC are shown in Table 4.

A. LANE KEEPING TEST

The lane keeping performance are compared in terms of chattering and lateral offset error. As illustrated in Fig.9, there is some chattering in the steering angle with the constant SMC, a little chattering with the adaptive SMC, and almost no chattering with the proposed SMC. The chattering phenomena are seen more clearly in the steering rate when driving on the curved section. The proposed controller provides stable steering input with no chattering mainly because the modeling errors are compensated and the controller gain is relatively small.

$$RMSE = \sqrt{\sum_{i=1}^{n} \frac{(\hat{y}_i - y_i)^2}{n}} \tag{34}$$

The lateral offset error in lane keeping is very important for autonomous bus because of larger width and overhang

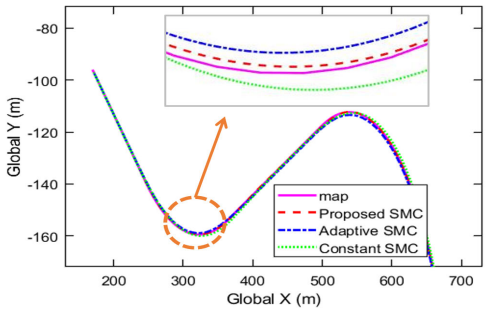

FIGURE 11. Comparison of cornering trajectories.

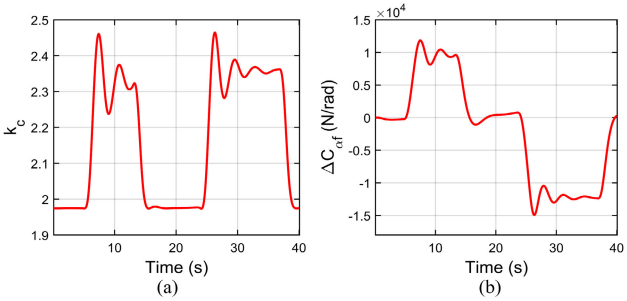

FIGURE 12. Calculated stiffness gain and cornering stiffness bias.

TABLE 5. Root mean square error of control.

RMSE	Constant SMC [27]	Adaptive SMC [29]	Proposed SMC
Lateral position(m)	0.661	0.257	0.083
Heading(deg)	4.641	3.896	3.037

of the bus. Figure 10 shows that the proposed controller significantly outperforms the other controllers. In the curved section, lateral offset errors of the constant SMC and the adaptive SMC exceed 0.5 m, but the lateral error of the proposed SMC is less than 0.3 m. In addition, the proposed SMC shows the smallest heading error than the other SMCs, suggesting that the controlled bus is most likely to stay in the lane. Figure 11 illustrates lateral offset error of each controller with respect to the centerline. The root mean square values of lateral offset error and heading error are listed Table 5 for each controller.

During the simulation, the stiffness gain and the cornering stiffness bias are calculated using (20) and their values are shown in Fig.12. These results demonstrate how the estimated disturbance is used to update the modeling errors in real-time.

B. MODEL UNCERTAINTY TEST

The control performnance against model uncertainty is verified when the bus weight changes by 20%, 50%, and 100%, respectively. The maximum values of the lateral offset error are compared for the three SMC controllers in

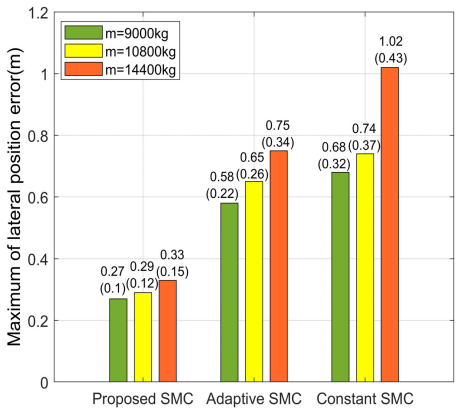

FIGURE 13. Lateral offset error with weight change.

Fig.13. Their RMSE values are also listed in parentheses. While the proposed SMC controller produced a small increase to 0.33 m when mass is doubled, the adaptive SMC showed a large increase to 0.75 m and the constant SMC showed even larger increase to 1.02 m. Therefore, it can be confirmed that the proposed controller not only improves lane keeping performance compared to the conventional SMC controllers, but also improves robustness against the model uncertainty.

V. EXPERIMENTAL TEST

Experimental tests were conducted to verify the lateral control performance of autonomous bus. The test site is shown in Fig.14 where GPS trajectories of the bus are compared with the digital map to evaluate the lane keeping performance. During the experiment, five people, including the driver, boarded the autonomous bus. Figure 15.(a) shows the picture of the test bus which was modified for autonomous driving and Figure 15.(b) depicts the overall sensor and hardware configuration. Lidar and Radar sensors are installed at front and rear for obstacle detection and a vision sensor is utilized for lane detection. In addition, a DGPS (Differential Global Positioning System) sensor is mounted on the top of the bus to track its location in real time. The algorithm of the proposed SMC controller is embedded into the RCP (Rapid Control Prototyping) device for real-time testing and all the sensor data is stored in the embedded PC through CAN network.

The vehicle parameters in Table 2 are used again for the proposed controller in experiments. The look-ahead distance is set by considering the speed and time delay in control. The look-ahead distance should increase with speed because the side slip angle increases with speed and the increase in side slip results in bigger heading error. The time delay in control includes the latency of the embedded PC, CAN network delay and the actuator delay of the steering wheel. Based on the repeated experiments, the look-ahead distance is set to change from 10 m to 30 m.

FIGURE 14. The test site for bus driving test.

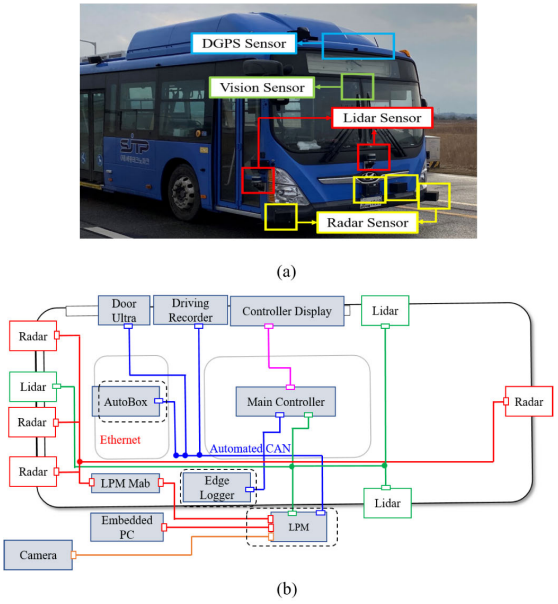

FIGURE 15. Modified bus for self-driving tests (a) Front view of the modified bus (b) Overall sensor and hardware configuration.

TABLE 6. Lateral offset and Heading errors in experiments.

	Human driver	Proposed control
Lateral position(m)	0.33(0.0724)	0.12(0.0243)
Heading(deg)	1.51(0.3627)	1.15(0.3237)

A. LANE KEEPING TEST

The lane keeping experiment is conducted using the proposed control system. The track is composed of straight and curved sections similarly to the simulation environment. Total driving time is 5 minutes, and the average velocity is kept constant at 50 km/h through the in-built cruise controller of the bus. A skilled human driver runs on the same track at 50 km/h as illustrated in Fig.16. The lateral offset error and heading error are compared in Fig.17 and Fig.18, respectively. The proposed control system performs better lane keeping maneuver than the human driver in terms of centering performance.

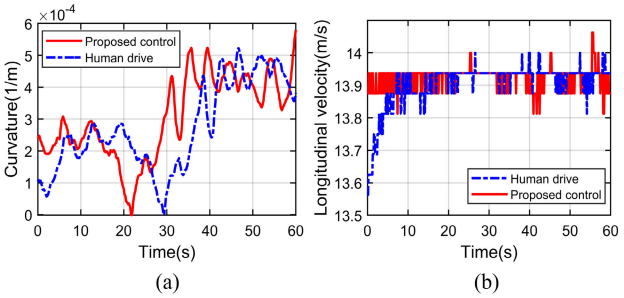

FIGURE 16. Recorded data of the proposed control system and human driver (a) Lane curvature. (b) Longitudinal velocity.

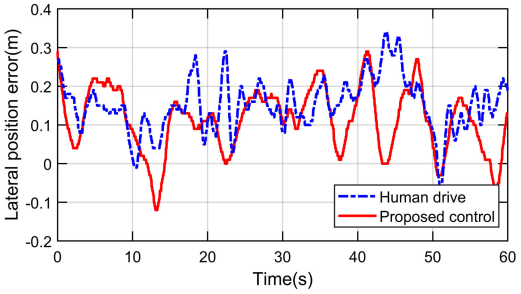

FIGURE 17. Lateral offset errors in experiments.

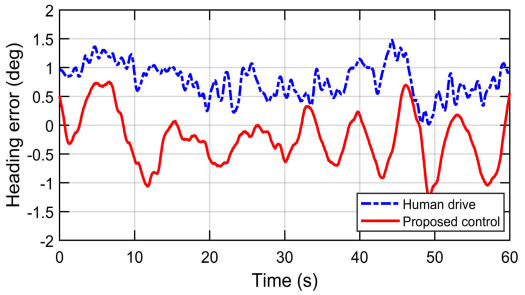

FIGURE 18. Heading errors in experiments.

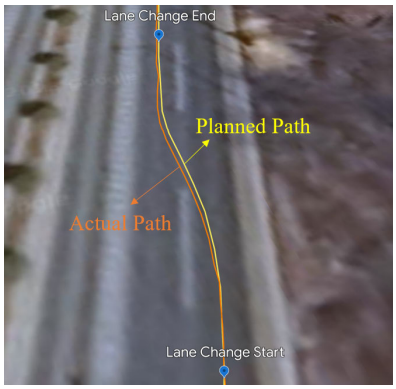

FIGURE 19. Actual and planned lane change trajectories in experiments.

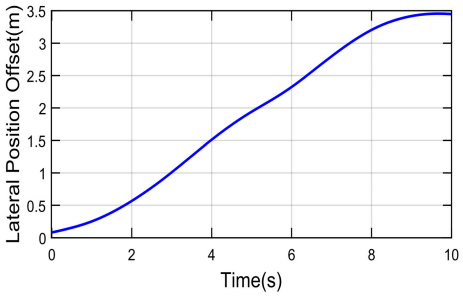

FIGURE 20. Lateral displacement data in lane change test.

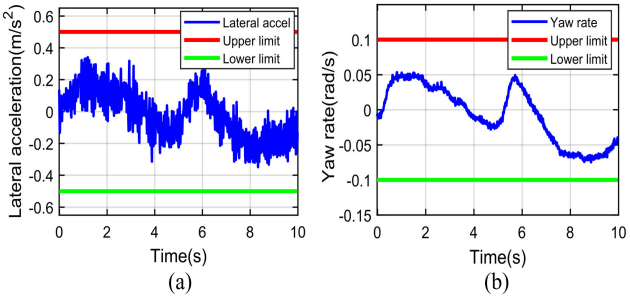

FIGURE 21. Lateral acceleration and yaw rate during lane change experiments.

The maximum lateral offset and heading errors are compared in Table 6 for the human driver and the proposed control system. The RMSE values are also listed in parentheses. The maximum error of the lateral offset from the proposed controller are about 63% smaller than the human driver. The human driver, unlike the control system, does not maintain a consistent look-ahead distance. Instead, the driver seeks to maintain centering by prioritizing road curvature on a curved track, which can result in bias in lateral position and heading.

B. LANE CHANGE TEST

The lane change experiment is conducted on a straight road with the longitudinal velocity at 40 km/h. The lane change path is generated by the optimization process and the sampling-based re-routing. After the bus moved into the next lane, the lane change maneuver is terminated and switched back to the lane keeping maneuver. During the mode-transition process, interpolation between lane change and lane keeping is utilized to prevent rapid changes in the path.

Figure 19 depicts the real-time generation of a lane change path by the Path Planner module during the Lane Change field test. In order to express the planned path in GPS coordinates, it is transformed from the vehicle coordinate system using the autonomous bus' current position as the reference. The path is mapped onto Google Earth, showing the lane change performance of the autonomous bus as recorded by the DGPS module. The lane change maneuver is designed to laterally move the vehicle by 3.5m, equivalent to the lane width, from the centerline of the current lane. This figure provides visual evidence of the successful tracking of the lane change maneuvering by the controller, as intended by

the Path Planner. Additionally, Figure 20 illustrates the lateral displacement data to assess the control system' performance in achieving the desired lane change. Figure 20 also shows the smoothness of the transition process between the lane change and lane keeping maneuvers without lane departure. The experimental results demonstrate that lateral acceleration and yaw rate constraints are satisfied within the bounds as illustrated in Fig.21.

VI. CONCLUSION

In this paper, a lateral control system for autonomous bus is developed such that robust control performance is enhanced with respect to model uncertainties and that the dynamic constraints of the bus is considered. Model uncertainties due to weight change and speed in bus are estimated based on the disturbance observer and used to update the cornering stiffness at front and rear wheels in real time. The optimal path planning and search-based planning methods are combined to generate a trajectory to prevent lane departure and to minimize lateral jerk. The Sliding Mode Controller (SMC) is designed based on the updated model to ensure the control performance in lateral motion of autonomous bus. Simulation results demonstrate that the proposed lateral control system provides reduced chattering, improved lane keeping and robust performance than the conventional SMC controllers. Furthermore, experimental results with the proposed lateral control system showed better lane keeping performance than an expert human driver and achieves smooth lane change maneuvering while satisfying the dynamic constraints set by the path planner. In future research, the model uncertainties will be further investigated in experiments with varying speed and weight to validate the proposed control system in path following performance. In addition, other control approaches according to the curvature of the lane will be further studied for the stability and ride comfort of autonomous buses.

APPENDIX A VEHICLE PARAMETERS

The vehicle parameters used in (17) are given as follows:

$$\bar{a}_{22} = -\frac{2\bar{C}_{af}(1+k_c)}{mV_x}, \bar{a}_{23} = \frac{2\bar{C}_{af}(1+k_c)}{m}$$
$$\bar{a}_{24} = \frac{2\bar{C}_{af}(-l_f+k_c\cdot l_r)}{mV_x}, \bar{a}_{42} = \frac{2\bar{C}_{af}(-l_f+k_c\cdot l_r)}{I_zV_x}$$
$$\bar{a}_{43} = \frac{2\bar{C}_{af}(l_f-k_c\cdot l_r)}{I_z}, \bar{a}_{44} = \frac{-2\bar{C}_{af}({l_f}^2+k_c\cdot {l_r}^2)}{I_zV_x}$$
$$\bar{b}_2 = \frac{2\bar{C}_{af}}{m}, \bar{b}_4 = \frac{2\bar{C}_{af}\cdot l_f}{I_z}$$
$$\bar{c}_2 = \frac{2\bar{C}_{af}(-l_f+k_c\cdot l_r)}{mV_x} - V_x, \bar{c}_4 = \frac{-2\bar{C}_{af}({l_f}^2+k_c\cdot {l_r}^2)}{I_zV_x}$$
$$\Delta a_{22} = -\frac{2\Delta C_{af}(1+k_c)}{mV_x}, \Delta a_{23} = \frac{2\Delta C_{af}(1+k_c)}{m}$$
$$\Delta a_{24} = \frac{2\Delta C_{af}(-l_f+k_c\cdot l_r)}{mV_x}, \Delta a_{42} = \frac{2\Delta C_{af}(-l_f+k_c\cdot l_r)}{I_zV_x}$$
$$\Delta a_{43} = \frac{2\Delta C_{af}(l_f-k_c\cdot l_r)}{I_z}, \Delta a_{44} = -\frac{2\Delta C_{af}({l_f}^2+k_c\cdot {l_r}^2)}{I_zV_x}$$
$$\Delta b_2 = \frac{2\Delta C_{af}}{m}, \Delta b_4 = \frac{2\Delta C_{af}\cdot l_f}{I_z}$$
$$\Delta c_2 = \frac{2\Delta C_{af}(-l_f+k_c\cdot l_r)}{mV_x}, \Delta c_4 = -\frac{2\Delta C_{af}({l_f}^2+k_c\cdot {l_r}^2)}{I_zV_x}$$

REFERENCES

[1] H. Sjafrie, *Introduction to Self-Driving Vehicle Technology*. Boca Raton, FL, USA: CRC Press, 2019.
[2] J. Stilgoe, "How can we know a self-driving car is safe?" *Ethics Inf. Technol.*, vol. 23, no. 4, pp. 635–647, Dec. 2021.
[3] J. Ackermann, D. Odenthal, and T. Bünte, "Advantages of active steering," in *Proc. ISATA*, 1999, pp. 263–270.
[4] L. Yu, D. Kong, X. Shao, and X. Yan, "A path planning and navigation control system design for driverless electric bus," *IEEE Access*, vol. 6, pp. 53960–53975, 2018.
[5] B. Arifin, B. Y. Suprapto, S. A. D. Prasetyowati, and Z. Nawawi, "The lateral control of autonomous vehicles: A review," in *Proc. Int. Conf. Electr. Eng. Comput. Sci. (ICECOS)*, Oct. 2019, pp. 277–282.
[6] R. C. Coulter, "Implementation of the pure pursuit path tracking algorithm," Robot. Inst., Carnegie-Mellon Univ., Pittsburgh, PA, USA, Tech. Rep. CMU-RI-TR-92-01, 1992.
[7] S. Thrun et al., "Stanley: The robot that won the DARPA grand challenge," *J. Field Robot.*, vol. 23, no. 9, pp. 661–692, 2006.
[8] H. F. Grip, L. Imsland, T. A. Johansen, J. C. Kalkkuhl, and A. Suissa, "Vehicle sideslip estimation," *IEEE Control Syst. Mag.*, vol. 29, no. 5, pp. 36–52, Oct. 2009.
[9] Y. Zhang, A. Khajepour, and Y. Huang, "Multi-axle/articulated bus dynamics modeling: A reconfigurable approach," *Vehicle Syst. Dyn.*, vol. 56, no. 9, pp. 1315–1343, Sep. 2018.
[10] R. Rajamani, *Vehicle Dynamics and Control*. New York, NY, USA: Springer, 2011.
[11] D. L. Ossig, S. A. Speidel, and O. Sawodny, "Parameter uncertainties influencing vehicle lateral dynamics steady state applications," in *Proc. IEEE Int. Conf. Ind. Technol. (ICIT)*, Feb. 2020, pp. 881–886.
[12] S. Kim, K. Shin, C. Yoo, and K. Huh, "Development of algorithms for commercial vehicle mass and road grade estimation," *Int. J. Automot. Technol.*, vol. 18, no. 6, pp. 1077–1083, Dec. 2017.
[13] Y. F. Lian, Y. Zhao, L. L. Hu, and Y. T. Tian, "Cornering stiffness and sideslip angle estimation based on simplified lateral dynamic models for four-in-wheel-motor-driven electric vehicles with lateral tire force information," *Int. J. Automot. Technol.*, vol. 16, no. 4, pp. 669–683, Aug. 2015.
[14] M. Shi, H. He, J. Li, M. Han, and N. Zhou, "Path planning and following control of autonomous bus under time-varying parameters against parametric uncertainties and external disturbances," *IEEE Trans. Veh. Technol.*, vol. 71, no. 7, pp. 7057–7070, Jul. 2022.
[15] S. Han, J. Ryu, G. Kim, J. Choi, and K. Huh, "Emergency steering collision avoidance and path tracking system for city bus considering yaw response," in *Proc. 22nd Int. Conf. Control, Autom. Syst. (ICCAS)*, Nov. 2022, pp. 1630–1635.
[16] R. Marino, S. Scalzi, and M. Netto, "Nested PID steering control for lane keeping in autonomous vehicles," *Control Eng. Pract.*, vol. 19, no. 12, pp. 1459–1467, Dec. 2011.
[17] C. Piao, X. Liu, and C. Lu, "Lateral control using parameter self-tuning LQR on autonomous vehicle," in *Proc. Int. Conf. Intell. Comput., Autom. Syst. (ICICAS)*, Dec. 2019, pp. 913–917.
[18] A. Mohammadzadeh and H. Taghavifar, "A novel adaptive control approach for path tracking control of autonomous vehicles subject to uncertain dynamics," *Proc. Inst. Mech. Eng. D, J. Automobile Eng.*, vol. 234, no. 8, pp. 2115–2126, Jul. 2020.
[19] Z. Chu, Y. Sun, C. Wu, and N. Sepehri, "Active disturbance rejection control applied to automated steering for lane keeping in autonomous vehicles," *Control Eng. Pract.*, vol. 74, pp. 13–21, May 2018.
[20] S. Zhu, S. Y. Gelbal, B. Aksun-Guvenc, and L. Guvenc, "Parameter-space based robust gain-scheduling design of automated vehicle lateral control," *IEEE Trans. Veh. Technol.*, vol. 68, no. 10, pp. 9660–9671, Oct. 2019.
[21] X. Jin, Q. Wang, Z. Yan, and H. Yang, "Nonlinear robust control of trajectory-following for autonomous ground electric vehicles with active front steering system," *AIMS Math.*, vol. 8, no. 5, pp. 11151–11179, 2023.

[22] A. Katriniok and D. Abel, "LTV-MPC approach for lateral vehicle guidance by front steering at the limits of vehicle dynamics," in *Proc. 50th IEEE Conf. Decis. Control Eur. Control Conf.*, Dec. 2011, pp. 6828–6833.
[23] M. Bujarbaruah, X. Zhang, H. E. Tseng, and F. Borrelli, "Adaptive MPC for autonomous lane keeping," 2018, *arXiv:1806.04335*.
[24] P. Falcone, F. Borrelli, H. E. Tseng, J. Asgari, and D. Hrovat, "Linear time-varying model predictive control and its application to active steering systems: Stability analysis and experimental validation," *Int. J. Robust Nonlinear Control*, vol. 18, no. 8, pp. 862–875, 2008.
[25] K. D. Young, V. I. Utkin, and U. Ozguner, "A control engineer's guide to sliding mode control," *IEEE Trans. Control Syst. Technol.*, vol. 7, no. 3, pp. 328–342, May 1999.
[26] Y. Shtessel et al., *Sliding Mode Control and Observation*, vol. 10. New York, NY, USA: Springer, 2014.
[27] H. Du, Z. Man, J. Zheng, A. Cricenti, H. Wang, and Y. Zhao, "A novel sliding mode control for lane keeping in road vehicles," in *Proc. Int. Conf. Adv. Mech. Syst. (ICAMechS)*, Nov. 2016, pp. 289–294.
[28] D. Ao, W. Huang, P. K. Wong, and J. Li, "Robust backstepping super-twisting sliding mode control for autonomous vehicle path following," *IEEE Access*, vol. 9, pp. 123165–123177, 2021.
[29] A. Norouzi, R. Kazemi, and S. Azadi, "Vehicle lateral control in the presence of uncertainty for lane change maneuver using adaptive sliding mode control with fuzzy boundary layer," *Proc. Inst. Mech. Eng. I, J. Syst. Control Eng.*, vol. 232, no. 1, pp. 12–28, Jan. 2018.
[30] P. Hingwe and M. Tomizuka, "Experimental study of chatter free sliding mode control for lateral control of commuter buses in AHS," UC Berkeley, California Partners Adv. Transp. Technol., Tech. Rep. UCB-ITS-PRR-96-31, 1996.
[31] T. Nguyen, N. NguyenDinh, B. Lechner, and Y. D. Wong, "Insight into the lateral ride discomfort thresholds of young-adult bus passengers at multiple postures: Case of Singapore," *Case Stud. Transp. Policy*, vol. 7, no. 3, pp. 617–627, Sep. 2019.
[32] J.-S. Jo, S.-H. You, J. Y. Joeng, K. I. Lee, and K. Yi, "Vehicle stability control system for enhancing steerabilty, lateral stability, and roll stability," *Int. J. Automot. Technol.*, vol. 9, no. 5, pp. 571–576, Oct. 2008.
[33] L. Liu, G. Tan, H. Ling, P. Zeng, C. Li, and C. Ou, "Research on vehicle lane change based on vehicle speed planning," SAE Tech. Paper 2021-01-0162, 2021.
[34] I. A. Ntousakis, I. K. Nikolos, and M. Papageorgiou, "Optimal vehicle trajectory planning in the context of cooperative merging on highways," *Transp. Res. C, Emerg. Technol.*, vol. 71, pp. 464–488, Oct. 2016.
[35] M. Werling, S. Kammel, J. Ziegler, and L. Gröll, "Optimal trajectories for time-critical street scenarios using discretized terminal manifolds," *Int. J. Robot. Res.*, vol. 31, no. 3, pp. 346–359, Mar. 2012.
[36] C. Sierra, E. Tseng, A. Jain, and H. Peng, "Cornering stiffness estimation based on vehicle lateral dynamics," *Vehicle Syst. Dyn.*, vol. 44, no. sup1, pp. 24–38, Jan. 2006.
[37] D. D. MacInnis, W. E. Cliff, and K. W. Ising, "A comparison of moment of inertia estimation techniques for vehicle dynamics simulation," *SAE Trans.*, pp. 1557–1575, 1997.
[38] S. Li, J. Yang, W.-H. Chen, and X. Chen, *Disturbance Observer-Based Control: Methods and Applications*. Boca Raton, FL, USA: CRC Press, 2014.
[39] K. Erbatur and A. Kawamura, "Chattering elimination via fuzzy boundary layer tuning," in *Proc. IEEE 28th Annu. Conf. Ind. Electron. Soc. (IECON)*, vol. 3, Nov. 2002, pp. 2131–2136.
[40] V. I. Utkin and A. S. Poznyak, "Adaptive sliding mode control with application to super-twist algorithm: Equivalent control method," *Automatica*, vol. 49, no. 1, pp. 39–47, Jan. 2013.
[41] *Trucksim 8.1*, Mech. Simul., Ann Arbor, MI, USA, 2011.

HUN HWANGBO received the B.S. degree in mechanical engineering from Inha University, Seoul, South Korea, in 2021. He is currently pursuing the master's degree with the Department of Future Mobility, Hanyang University. His research interests include longitudinal and lateral control of autonomous vehicles with robust control techniques, AI technology for trajectory prediction of surrounding objects, and search-based optimal path planning.

JAEUN RYU received the B.S. degree in automotive engineering from Hanyang University, Seoul, South Korea, in 2021. He is currently pursuing the master's degree with the Department of Automotive Engineering. His research interests include decision-making, motion planning, and control of autonomous vehicles, which is making maneuvering decisions via the surrounding environment and planned path.

SANGWON HAN received the B.S. degree in automotive engineering from Hanyang University, Seoul, South Korea, in 2018. He is currently pursuing the Ph.D. degree with the Department of Automotive Engineering (Automotive-Computer Convergence). His research interests include planning and control of commercial vehicles, which is path planning considering surrounding vehicles or obstacles in large vehicles and developing optimal control systems through analysis of the dynamic characteristics of vehicles.

KUNSOO HUH (Member, IEEE) received the Ph.D. degree from the University of Michigan, Ann Arbor, MI, USA, in 1992. He is currently a Professor with the Department of Automotive Engineering, Hanyang University, Seoul, South Korea. His research interests include machine monitoring and control, with emphasis on their applications to vehicular systems. His current research interests include sensor-based active safety systems, V2X-based safety systems, autonomous vehicle control, and AI applications in autonomous vehicles.